Dalton Transactions

PAPER

View Article Online
View Journal | View Issue

Cite this: *Dalton Trans.*, 2016, **45**, 19408

An unusual co-crystal $[(\mu_2\text{-dcpm})Ag_2(\mu_2\text{-}O_2CH)(\eta^2\text{-}NO_3)]_2\cdot[(\mu_2\text{-dcpm})_2Ag_4(\mu_2\text{-}NO_3)_4]$ and its connection to the selective decarboxylation of formic acid in the gas phase†

Athanasios Zavras, Jonathan M. White and Richard A. J. O'Hair*

Received 23rd September 2016,
Accepted 14th November 2016

DOI: 10.1039/c6dt03700c

www.rsc.org/dalton

ESI/MS of an acetonitrile solution containing a mixture of $AgNO_3$: bis(dicyclohexylphosphino)methane (dcpm, L) : NaO_2CH in a molar ratio of 2 : 1 : 1 gave an abundant peak due to $[LAg_2(O_2CH)]^+$ and a minor peak assigned as $[L_2Ag_4(O_2CH)_3]^+$. When this acetonitrile solution was frozen and layered with diethyl ether and left undisturbed for six days, crystalline material suitable for X-ray crystallography was identified and separated from amorphous solids. Single crystal X-ray diffraction revealed an unusual co-crystal consisting of two discrete tetranuclear silver clusters $[(\mu_2\text{-dcpm})Ag_2(\mu_2\text{-}O_2CH)(\eta^2\text{-}NO_3)]_2\cdot[(\mu_2\text{-dcpm})_2Ag_4(\mu_2\text{-}NO_3)_4]$. While all of the coordinated formates in $[LAg_2(O_2CH)]^+$ and $[L_2Ag_4(O_2CH)_3]^+$ can be decarboxylated in the gas-phase under conditions of collision induced dissociation, only the hydride $[LAg_2(H)]^+$ thus formed reacts with formic acid *via* protonation and liberation of H_2 to regenerate to formate, thereby closing a catalytic cycle for the selective decomposition of formic acid.

Introduction

Formic acid has emerged as one of the few organic liquids with potential for hydrogen storage applications.[1] In the absence of a catalyst, high temperatures are required for decarboxylation to release hydrogen from formic acid. Furthermore, this process is non-selective, being in competition with decomposition into water and carbon monoxide.[2] Thus there has been considerable interest in developing metal catalysts to selectively decarboxylate formic acid at low temperatures.[3]

We recently described a two-step catalytic cycle for the selective decomposition of formic acid into CO_2 and hydrogen in the gas phase (Scheme 1a, eqn (1)).[4] The crucial steps involve: (i) collision-induced dissociation (CID) of the binuclear bisphosphine silver formate, $[(L)Ag_2(O_2CH)]^+$ **1**, which liberates CO_2 and results in the formation of the coordinated hydride, $[(L)Ag_2(H)]^+$ **2**; (ii) an ion-molecule reaction (IMR) between **2** and formic acid to regenerate **1** *via* protonation of the coordinated hydride with concomitant liberation of H_2 (eqn (2)), thereby closing the catalytic cycle. Both resting states of the catalytic cycle were characterised by gas-phase IR and UV-Vis spectroscopy for the case of bis(diphenylphosphino)methane (dppm) ligand and were found to adopt the bidentate structures $[(\mu_2\text{-dppm})Ag_2(\mu_2\text{-}O_2CH)]^+$ **1a**, and $[(\mu_2\text{-dppm})Ag_2(\mu_2\text{-H})]^+$ **2a**. These gas phase results prompted variable temperature NMR experiments on a mixture of $AgBF_4$, dppm, sodium formate and formic acid, which revealed the formation of CO_2 and H_2 at 65 °C.

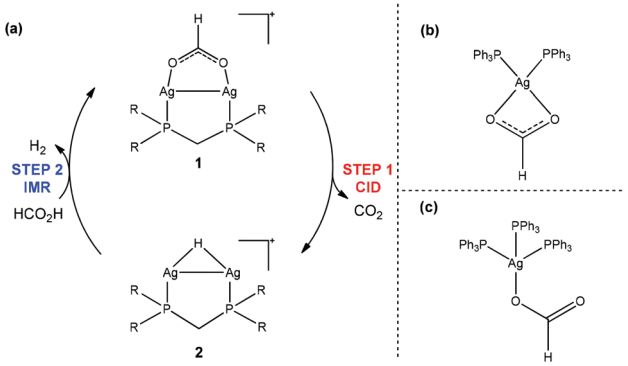

Scheme 1 (a) Catalytic cycle for the selective decarboxylation of formic acid; previous crystal structures of phosphine ligated silver formates: (b) $[(Ph_3P)_2Ag(\eta^2\text{-}O_2CH)]$[5] and (c) $[(Ph_3P)_3Ag(O_2CH)]$.[6] R = Ph and **1a** and **2a** (ref. 4); R = Cy and **1b** and **2b** (this work).

$$[LAg_2(O_2CH)]^+ \rightarrow [LAg_2(H)]^+ + CO_2 \quad (1)$$

$$[LAg_2(H)]^+ + HO_2CH \rightarrow [LAg_2(H)]^+ + H_2 \quad (2)$$

School of Chemistry and Bio21 Institute of Molecular Science and Biotechnology, The University of Melbourne, Melbourne, Victoria 3010, Australia.
E-mail: rohair@unimelb.edu.au

†Electronic supplementary information (ESI) available: Asymmetric unit of **3**; ion-molecule kinetics for reaction of $[LAg_2H]^+$, **2b**, with formic acid; crystallographic information for **3**. CCDC 1505745. For ESI and crystallographic data in CIF or other electronic format see DOI: 10.1039/c6dt03700c

Since the formate complex, **1**, represents the key entry point into the catalytic cycle, we were interested in determining its structure *via* X-ray crystallography. While X-ray crystallographic studies have characterised the structures of mononuclear silver phosphine formate complexes (Scheme 1b and c)[5,6] and several silver phosphine carboxylate clusters,[7] no cationic structures with the required 2 : 1 : 1 stoichiometry for Ag : bisphosphine : formate have been published. Indeed, it appears that $[(\mu_2\text{-dppm})_2Cu_2(\mu_2\text{-}O_2CCH_3)]BF_4$ and $[(\mu_2\text{-dppm})_2$(4-vinyl-pyridine)$Cu_2(\mu_2\text{-}O_2CH)]NO_3$ are the only cationic binuclear bisphosphine coinage metal carboxylates to have been characterised by X-ray crystallography.[8] Here we report the results of an attempt to form crystals with the required stoichiometry and ligand binding modes related to structure **1**. We also describe the results of ESI multistage mass spectrometry experiments on solutions of this stoichiometry aimed at examining what cations are formed and to provide a link to related gas-phase catalytic cycles for the selective decomposition of formic acid.

Experimental section

Chemicals

Chemicals from the following suppliers were used without further purification: Aldrich: (i) bis(dicyclohexylphosphino) methane (dcpm, L) (97%), (ii) silver(I) tetrafluoroborate ($AgBF_4$) (98%), (iii) sodium formate (NaO_2CH, 99%). Ajax Finechem: (iv) formic acid (HCO_2H, 99%), (v) silver(I) nitrate ($AgNO_3$). Merck: (vi) acetronitrile (HPLC grade).

Preparation of $[(\mu_2\text{-dcpm})Ag_2(\mu_2\text{-}O_2CH)(\eta^2\text{-}NO_3)]_2\cdot[(\mu_2\text{-dcpm})_2Ag_4(\mu_2\text{-}NO_3)_4]$ 3

$AgNO_3$ (0.017 g, 0.10 mmol) and bis(dicyclohexylphosphino) methane (0.020 g, 0.05 mmol) were added to a 10 mL glass vial with a screw-cap. Acetonitrile (5 cm^3) was added to the vial and the solution was sonicated for 1 minute. Formic acid was added in excess and the solution was sonicated for a further 1 minute. NaO_2CH (0.004 g, 0.05 mmol) was added to the solution under stirring until dissolved, *ca.* 5 minutes. The solution was frozen with liquid nitrogen and layered with diethylether. The screw-cap was immediately fitted and sealed with Teflon and parafilm tape. The vial was wrapped in aluminium foil and left undisturbed for 6 days to afford crystals suitable for X-ray crystallography. Although some decomposition and silver mirrors were observed, crystals suitable for X-ray crystallography were manually collected by sorting through the solid material suspended in paraffin under a microscope.

X-ray crystallography

Intensity data for compound **3** was collected on an Oxford Diffraction SuperNova CCD diffractometer using Cu-Kα radiation, the temperature during data collection was maintained at 130.0(1) using an Oxford Cryostream cooling device. The structure was solved by direct methods and difference Fourier synthesis.[9] The thermal ellipsoid plot was generated using the program ORTEP-3 [10] integrated within the WINGX[11] suite of programs.

Mass spectrometry

Mass spectra were recorded using a Thermo Finnigan linear ion trap (LTQ) mass spectrometer modified to allow ion-molecule reactions to be carried out. The silver clusters prepared in the condensed phase were introduced into the mass spectrometer *via* a syringe pump set at a flow rate of 5 μL min^{-1} to the ESI capillary. The ESI conditions used, for optimum intensity of the target ions, typically were: spray voltage, 4.2–5.0 kV, capillary temperature, 250 °C, nitrogen sheath gas pressure, 5 (arbitrary units), capillary voltage. CID experiments were carried out by mass selecting the entire isotope cluster with a window of 8 *m*/*z* and applying an activation energy between 15% and 25% NCE to allow collisions with the helium bath gas. An activation (*Q*) of 0.25 and activation time of 30 ms were used. IMR were carried by injecting formic acid into the helium bath gas, and rates were measured by varying the reaction time, as described previously.[12] Under IMR conditions, collisions with the helium bath gas quasi-thermalizes the ions to room temperature.[12c] The ADO average-dipole orientation theory rate coefficient was calculated using the COLRATE program.[13]

Results and discussion

ESI/MS to investigate clusters formed in solution from silver salts with dcpm HCOOH and NaO_2CH

ESI/MS was used to monitor the reactions of silver salts with bisphosphine ligand and sodium formate in an effort to identify suitable conditions for the synthesis of a ligand protected silver formate cluster. The reaction of $AgBF_4$: dcpm : NaO_2CH in a molar ratio of 2 : 1 : 1 yielded abundant $[LAg_2(O_2CH)]^+$ (*m*/*z* 669, Fig. 1a) in agreement with the stoichiometric conditions applied in the synthesis. The related dinuclear complex $[LAg_2(O_2CH)]^+$ was observed for ESI/MS of solutions containing dppm instead of dcpm (data not shown). Although ESI/MS has been previously used to direct the synthesis of silver clusters[14] and the observation of abundant $[LAg_2(O_2CH)]^+$ showed promise for the condensed phase synthesis of a dinuclear silver formate, all attempts failed to produce crystalline material associated with a discrete cluster of the form of $[LAg_2(O_2CH)]X$, where L = dcpm or dppm, X = a non-coordinating anion BPh_4^- and BF_4^-. Instead, slowly diffusing solutions resulted in the formation of silver mirrors on the glass vial and in amorphous products of decomposition.

ESI/MS of an acetonitrile solution of $AgNO_3$: dcpm : NaO_2CH in a molar ratio of 2 : 1 : 1 also gave an abundant peak due to $[LAg_2(O_2CH)]^+$ (*m*/*z* 669, Fig. 1b). A minor peak of *ca.* 1.25% observed at *m*/*z* 1383 was assigned as $[L_2Ag_4(O_2CH)_3]^+$.

When an acetonitrile solution of $AgNO_3$: dcpm : NaO_2CH in a molar ratio of 2 : 1 : 1 was frozen and layered with diethyl ether and left undisturbed for six days, a mixture of amorphous and crystalline solids were observed at the solvent interface. There were two types of amorphous material. One was a grey flocculant material and the other was a blackened solid. The solid material was suspended in paraffin and examined

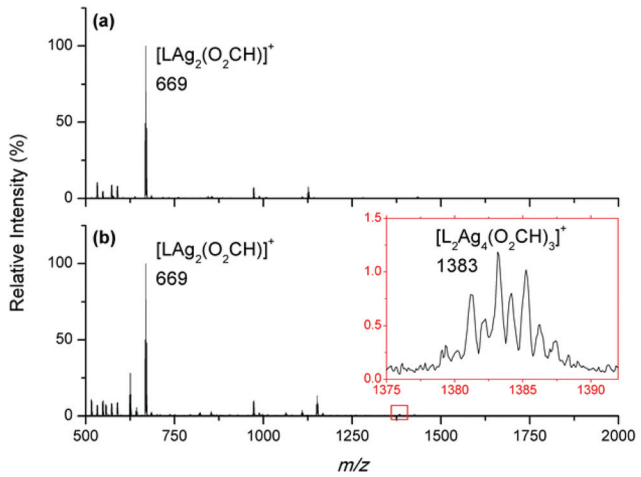

Fig. 1 Positive-ion LTQ ESI/MS of acetonitrile solutions of silver formate clusters prepared from: (a) $AgBF_4$: dcpm : HCOOH : NaO_2CH (2 : 1 : 1 : 1) and (b) $AgNO_3$: dcpm : HCOOH : NaO_2CH (2 : 1 : 1 : 1). Solutions were diluted to 50 μm prior to ESI. L = dcpm = bis(dicyclohexylphosphino)methane. The *m*/*z* values shown are of the most intense peak arising from isotopic abundances of the atoms. Other ions formed in minor abundance are due to other ligated silver complexes formed by various combinations of Ag^+, solvent, dppm ligand (or in its oxidised formed) and anions. Their assignments are listed in ESI Table S1.†

under a light microscope to identify and manually separate crystalline material, from the amorphous solids, suitable for X-ray crystallography.

Structural characterization of $[(\mu_2\text{-dcpm})Ag_2(\mu_2\text{-}O_2CH)(\eta^2\text{-}NO_3)]_2\cdot[(\mu_2\text{-dcpm})_2Ag_4(\mu_2\text{-}NO_3)_4]$ (3) by X-ray crystallography

Single crystal X-ray diffraction revealed an unusual co-crystal[15] consisting of two discrete tetranuclear silver clusters $[(\mu_2\text{-dcpm})Ag_2(\mu_2\text{-}O_2CH)(\eta^2\text{-}NO_3)]_2\cdot[(\mu_2\text{-dcpm})_2Ag_4(\mu_2\text{-}NO_3)_4]$ (Fig. 2).‡ The former cluster has crystallographic inversion symmetry. When the asymmetric unit (Fig. S1†) is expanded, to show the crystal packing, the two clusters exhibit close intermolecular contacts between axial and equatorial hydrogen atoms from the cyclohexyl rings, from dcpm, on adjacent clusters (Table S1†). These van der Waals interactions likely provide a stabilising force as a template for the crystal packing of the clusters.

Structure of $[(\mu_2\text{-dcpm})Ag_2(\mu_2\text{-}O_2CH)(\eta^2\text{-}NO_3)]_2$

The structure of $[(\mu_2\text{-dcpm})Ag_2(\mu_3\text{-}O_2CH)(\eta^2\text{-}NO_3)]_2$ displays the typical μ_2-bridging of the short bite-angle ligand dcpm. Two structures in the CSD containing the "$(\mu_2\text{-dcpm})Ag_2$" structural motif exhibit short Ag–Ag contacts ranging from 2.889–2.959 Å, Ag–P bond distances are typically asymmetrical and range between 2.354–2.409 Å and the P–C–P angle ranges between 113.242–116.846°.[16] In comparison the Ag–Ag contacts of $[(\mu_2\text{-dcpm})Ag_2(\mu_2\text{-}O_2CH)(\eta^2\text{-}NO_3)]_2$ 3.2294(4) are significantly longer, however remain below the sum of the van der Waals radii (3.4 Å)[17] suggesting the possibility of argentophilic interactions.[18] The Ag–P contacts which range from 2.333 to 2.564 Å are typical, while the P–C–P angle of, 112.2(2)°, is more acute than previously reported, this is a reflection of the greater puckering of the (Ag_2 dcpm chelate ring). Opposing the dinuclear Ag–Ag edge lies a formato ligand with a μ_2-bridging coordination mode. The Ag–O contacts from the bridging formato ligand are asymmetrical with bond lengths of 2.161(3) and 2.288(4) Å. The collective μ_2-bridging dcpm and the formato ligands give a quasi-eight membered-ring ($Ag_2P_2C_2O_2$) with the silver atoms on opposing sides. The Ag(2) atom is chelated by an η^2-nitrato ligand, related binding has been observed by Mak and coworkers in a series of polymeric silver complexes and clusters.[19] The overall $[(\mu_2\text{-dcpm})Ag_2(\mu_2\text{-}O_2CH)(\eta^2\text{-}NO_3)]_2$ cluster is a centrosymmetric dimer of $[(\mu_2\text{-dcpm})Ag_2(\mu_2\text{-}O_2CH)(\eta^2\text{-}NO_3)]$ moieties which form a 4-membered (Ag–O–Ag–O) ring (Scheme 2a). A related four-membered Ag_2O_2 ring has previously been observed in a triphenylphosphine silver acetate complex $[(Ph_3P)_2Ag_2(\mu_2\text{-}O_2CCH_3)_2]_2$ (Scheme 2b). While the Ag–O distances linking the two halves of this cluster are similar, the the formate ligand displays shorter contacts to the silver atom, Ag(1)–O(1) 2.161(3) Å, than the acetate carboxylate ligand (Scheme 2b) (Table 1).

Structure of $[(\mu_2\text{-dcpm})_2Ag_4(\mu_2\text{-}NO_3)_4]$

An examination of the structure of the tetranuclear cluster $[(\mu_2\text{-dcpm})_2Ag_4(\mu_2\text{-}NO_3)_4]$ reveals that it can be considered as two L_2Ag_2 fragments held together by four nitrato ligands, giving rise to four fused eight membered rings (Scheme 3). Each L_2Ag_2 fragment adopts a quasi-staggered conformation. All four Ag–P bonds have comparable lengths, ranging 2.3473(10)–2.3255(9) Å. The Ag–O distances range between 2.217(3)–2.462(3) Å. The nitrato ligands bind in μ_2-bridging mode with the Ag–O bond length of ranging from 2.217(3)–2.462(3) Å. In comparison the Ag–O distance of a similar binding motif lies within the range 2.304–2.755 Å (Table 2).[19a,d,f]

Table S1† displays the intermolecular contacts at that exist between the two discrete clusters $[(\mu_2\text{-dcpm})Ag_2(\mu_2\text{-}O_2CH)(\eta^2\text{-}NO_3)]_2$ and $[(\mu_2\text{-dcpm})_2Ag_4(\mu_2\text{-}NO_3)_4]$. There are short distances between axial and equatorial hydrogen atoms on cyclohexyl rings of adjacent clusters. The nitrato ligand oxygen atoms also form short contacts with the methylene hydrogens and axial/equatorial cyclohexyl hydrogens.

Gas-phase reactivity of silver formate clusters

The observation of both $[LAg_2(O_2CH)]^+$ and $[L_2Ag_4(O_2CH)_3]^+$ clusters in the ESI/MS (Fig. 1b) provided an opportunity to examine whether these clusters take part in catalytic cycles for the selective decomposition of formic acid (*cf.* Scheme 1a). Since the first crucial step involves decarboxylation, $[L_2Ag_4(O_2CH)_3]^+$ (*m*/*z* 1383) was mass-selected and subjected to CID. A range of ionic products (Fig. 3) were observed, arising from three main reaction pathways: (i) decarboxylation, (ii) cluster fission and (iii) cluster fission coupled to ligand

‡The crystallographic information file for $[(\mu_2\text{-dcpm})Ag_2(\mu_2\text{-}O_2CH)(\eta^2\text{-}NO_3)]_2\cdot[(\mu_2\text{-dcpm})_2Ag_4(\mu_2\text{-}NO_3)_4]$ has been deposited at the Cambridge Crystallographic Data Centre and assigned the code: CCDC 1505745.

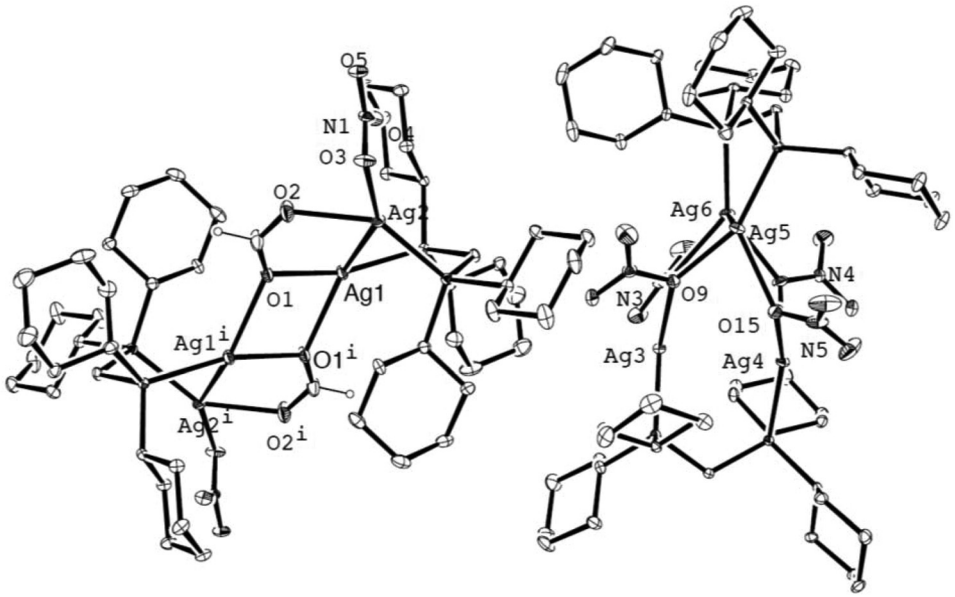

Fig. 2 ORTEP-3 representation of $[(\mu_2\text{-dcpm})Ag_2(\mu_2\text{-}O_2CH)(\eta^2\text{-}NO_3)]_2{\cdot}[(\mu_2\text{-dcpm})_2Ag_4(\mu_2\text{-}NO_3)]$, **3**. Displacement ellipsoids set at 20% probability level. Ag(1)–Ag(2): 3.2294(4)Å, Ag(1)–O(1): 2.485(3)Å, Ag(2)–O(2): 2.288(4)Å. Ag(3)–Ag(4): 3.3148(4)Å, Ag(5)–Ag(6): 3.1892(4)Å. Hydrogen atoms of the cyclohexyl rings have been omitted for clarity.

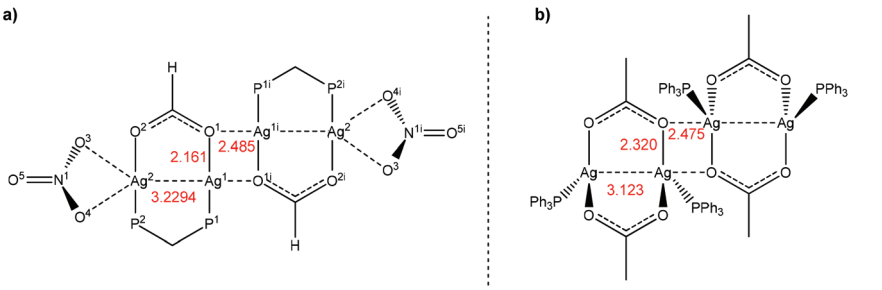

Scheme 2 A representation highlighting (a) the interaction between the two inversion-related of $[(\mu_2\text{-dcpm})Ag_2(\mu_2\text{-}O_2CH)(\eta^2\text{-}NO_3)]_2$, and (b) the similarity of $[(\mu_2\text{-dcpm})Ag_2(\mu_2\text{-}O_2CH)(\eta^2\text{-}NO_3)]_2$ to $[(Ph_3P)_2Ag_2(\mu_2\text{-}O_2CCH_3)_2]_2$.[20]

Table 1 Selected bond distances (Å) and angles (°) with esd's in parentheses for $[(\mu_2\text{-dcpm})Ag_2(\mu_2\text{-}O_2CH)(\eta^2\text{-}NO_3)]_2$

Ag(1)–Ag(2)	3.2294(4)	Ag(1)–O(1)–Ag(1[a])	102.89(13)
Ag(1)–O(1)	2.161(3)	O(1)–Ag(1)–O(1[a])	77.11(13)
Ag(1)–O(1[a])	2.485(3)	O(1)–Ag(1)–P(1)	162.80(9)
Ag(1)–O(1[a])	2.485(3)	O(2)–Ag(2)–P(2)	139.22(10)
Ag(1)–P(1)	2.3364(9)	O(1)–C(26)–O(2)	128.8(5)
Ag(2)–O(2)	2.288(4)	P(2)–C(13)–P(1)	112.2(2)
Ag(2)–O(3)	2.423(3)	O(3)–N(1)–O(4)	117.8(3)
Ag(2)–O(4)	2.536(6)	O(3)–N(1)–O(5)	121.1(3)
Ag(2)–P(2)	2.3591(10)	O(4)–N(1)–O(5)	121.0(3)
N(1)–O(3)	1.257(5)	P(2)–Ag(2)–O(3)	133.31(10)
N(1)–O(4)	1.256(5)	P(2)–Ag(2)–O(4)	131.15(8)
N(1)–O(5)	1.233(5)	Ag(1)–Ag(2)–O(3)	153.45(9)
C(26)–O(1)	1.269(6)	Ag(1)–Ag(2)–O(4)	115.42(7)
C(26)–O(2)	1.212(7)	N(1)–O(3)–Ag(2)	98.1(2)
C(13)–P(1)	1.847(4)	N(1)–O(4)–Ag(2)	92.6(2)
C(13)–P(2)	1.845(4)	O(1[a])–Ag(1)–Ag(2)	135.74(8)
Ag(1)–O(1[a])	2.485(3)	(O1[a])–Ag(1)–O(1)	77.11(13)
Ag(1)–P(1)	2.3364(9)	(O1[a])–Ag(1)–P(1)	120.07(8)

[a] Equivalent atom from adjacent unit cell.

loss. Sequential decarboxylation reactions give rise to $[L_2Ag_4(O_2CH)_2(H)]^+$ (m/z 1339, eqn (3)), $[L_2Ag_4(O_2CH)(H)_2]^+$ (m/z 1295, eqn (4)) and $[L_2Ag_4(H)_3]^+$ (m/z 1251, eqn (5)). The main fragmentation channel for the CID of $[L_2Ag_4(O_2CH)_3]^+$ (m/z 1383) is due to cluster fission *via* the loss of neutral $Ag_2(O_2CH)_2$ [21] to give $[L_2Ag_2(O_2CH)]^+$ (m/z 1077 eqn (6)). The next most abundant cluster is the hydride, $[L_2Ag_2(H)]^+$ (m/z 1033), which likely arises from combined cluster fission and decarboxylation (eqn (7)).

$$[L_2Ag_4(O_2CH)_3]^+ \rightarrow [L_2Ag_4(O_2CH)_2(H)]^+ + CO_2 \quad (3)$$

$$[L_2Ag_4(O_2CH)_3]^+ \rightarrow [L_2Ag_4(O_2CH)(H)_2]^+ + 2CO_2 \quad (4)$$

$$[L_2Ag_4(O_2CH)_3]^+ \rightarrow [L_2Ag_4(H)_3]^+ + 3CO_2 \quad (5)$$

$$[L_2Ag_4(O_2CH)_3]^+ \rightarrow [L_2Ag_2(O_2CH)]^+ + Ag_2(O_2CH)_2 \quad (6)$$

$$[L_2Ag_4(O_2CH)_3]^+ \rightarrow [L_2Ag_2(H)]^+ + Ag_2(O_2CH)_2 + CO_2 \quad (7)$$

Table 2 Selected bond distances (Å) and angles (°) with esd's in parentheses for $[(\mu_2\text{-dcpm})_2Ag_4(\mu_2\text{-}NO_3)_4]$

Ag(3)–Ag(4)	3.3148(4)	Ag(3)–Ag(4)–O(15)	89.64(10)
Ag(5)–Ag(6)	3.1892(4)	Ag(3)–O(9)–Ag(5)	138.21(15)
Ag(3)–O(6)	2.217(3)	Ag(4)–O(15)–Ag(5)	118.71(19)
Ag(3)–O(9)	2.462(3)	Ag(4)–Ag(3)–O(9)	84.17(2)
Ag(3)–P(3)	2.3473(10)	O(9)–Ag(5)–O(15)	89.64(10)
Ag(4)–O(15)	2.333(4)	Ag(3)–Ag(4)–O(12)	79.24(9)
Ag(4)–O(12)	2.367(3)	Ag(3)–O(6)–Ag(6)	127.42(15)
Ag(4)–P(4)	2.3380(9)	Ag(4)–O(12)–Ag(6)	141.16(16)
Ag(5)–O(15)	2.379(4)	Ag(4)–Ag(3)–O(6)	94.03(10)
Ag(5)–O(9)	2.236(3)	O(12)–Ag(6)–O(6)	81.02(13)
Ag(5)–P(5)	2.3368(9)	Ag(5)–Ag(6)–O(6)	95.24(8)
Ag(6)–O(6)	2.362(3)	Ag(5)–O(9)–Ag(3)	138.21(15)
Ag(6)–O(12)	2.324(4)	Ag(6)–O(6)–Ag(3)	127.42(15)
Ag(6)–P(6)	2.3255(9)	Ag(6)–Ag(5)–O(9)	77.29(13)
N(2)–O(6)	1.277(6)	O(6)–Ag(3)–O(9)	75.35(12)
N(2)–O(7)	1.281(7)	Ag(5)–Ag(6)–O(12)	71.71(11)
N(2)–O(8)	1.204(6)	Ag(5)–O(15)–Ag(4)	118.71(19)
N(3)–O(9)	1.280(5)	Ag(4)–O(12)–Ag(6)	141.16(16)
N(3)–O(10)	1.216(6)	Ag(6)–Ag(5)–O(15)	104.16(11)
N(3)–O(11)	1.232(5)	O(12)–Ag(4)–O(15)	82.26(15)
N(4)–O(12)	1.275(5)	P(3)–C(39)–P(4)	116.3(2)
N(4)–O(13)	1.231(6)	P(5)–C(64)–P(6)	113.6(2)
N(4)–O(14)	1.218(6)	Ag(3)–P(3)–C(39)	116.33(12)
N(5)–O(15)	1.257(6)	Ag(4)–P(4)–C(39)	119.04(12)
N(5)–O(16)	1.217(6)	Ag(5)–P(5)–C(64)	113.59
N(5)–O(17)	1.235(7)	Ag(6)–P(6)–C(64)	115.36(13)

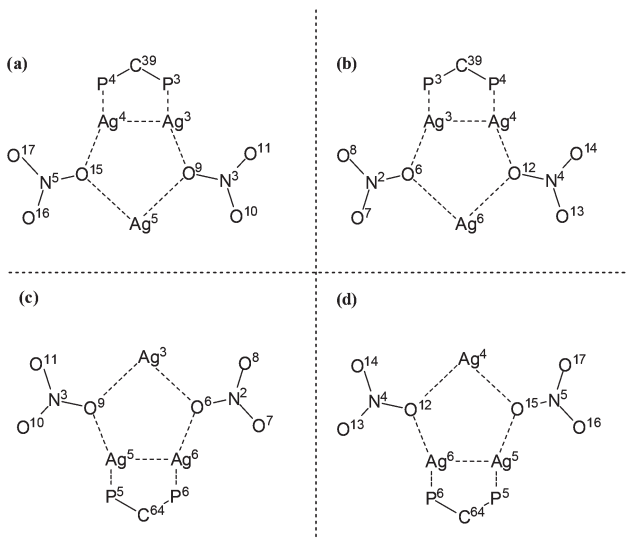

Scheme 3 A representation highlighting the four fused eight-membered rings of $[(\mu_2\text{-dcpm})_2Ag_4(\mu_2\text{-}NO_3)_4]$.

Ligand loss coupled to cluster fission drives the fragmentation of $[L_2Ag_4(O_2CH)_3]^+$ to $[LAg_2(O_2CH)]^+$ (*m*/*z* 669) *via* the neutral loss of $LAg_2(O_2CH)_2$ (eqn (8)). The related $[dcpmAg_2(O_2CF_3)_2]$ cluster with trifluroacetato ligands in place of the formato ligands has been observed.[16b] The dinuclear silver hydride $[LAg_2(H)]^+$ (*m*/*z* 625) is coupled to the loss of neutral $LAg_2(O_2CH)_2$ and CO_2 (eqn (9)).

$$[L_2Ag_4(O_2CH)_3]^+ \rightarrow [LAg_2(O_2CH)]^+ + LAg_2(O_2CH)_2 \quad (8)$$

$$[L_2Ag_4(O_2CH)_3]^+ \rightarrow [LAg_2(H)]^+ + LAg_2(O_2CH)_2 + CO_2 \quad (9)$$

$$[L_2Ag_4(O_2CH)_3]^+ \rightarrow [LAg]^+ + Ag_3(O_2CH)_3 \quad (10)$$

Mass selection followed by CID on $[L_2Ag_4(O_2CH)_2(H)]^+$ (*m*/*z* 1339, Fig. 3b) or $[L_2Ag_4(O_2CH)(H)_2]^+$ (*m*/*z* 1295, Fig. 3c) only gives rise to decarboxylation reactions (eqn (11)–(13)), with no cluster fission reactions being observed. Finally, the binuclear clusters $[L_2Ag_2(O_2CH)]^+$ (Fig. 3d) and $[LAg_2(O_2CH)]^+$ (Fig. 4a) also mainly undergo decarboxylation (eqn (14), eqn (1) and step 1 of Scheme 1). In the case of $[L_2Ag(O_2CH)]^+$ the branching ratio (BR) for decarboxylation is 95%, while the other minor channels do not involve fragmentation of the coordinated formate, but rather involve silver formate loss to give $[LAg]^+$ (*m*/*z* 517, BR = 1.8%) or loss of the protonated dppm ligand (*m*/*z* 409, BR = 3.2%).

$$[L_2Ag_4(O_2CH)_2(H)]^+ \rightarrow [L_2Ag_4(O_2CH)(H)_2]^+ + CO_2 \quad (11)$$

$$[L_2Ag_4(O_2CH)_2(H)]^+ \rightarrow [L_2Ag_4(H)_3]^+ + 2CO_2 \quad (12)$$

$$[L_2Ag_4(O_2CH)(H)_2]^+ \rightarrow [L_2Ag_4(H)_3]^+ + CO_2 \quad (13)$$

$$[L_2Ag_2(O_2CH)]^+ \rightarrow [L_2Ag_2(H)]^+ + CO_2 \quad (14)$$

Ion-molecule reactions of silver hydrides with formic acid

Since the next step of the catalytic cycle involves protonation of the coordinated hydride to liberate hydrogen and reform the formate complex (step 2 of Scheme 1a and eqn (2)), we next isolated each of the hydride complexes formed *via* CID and exposed them to formic acid inside the ion-trap. $[L_2Ag_4(O_2CH)_2(H)]^+$, $[L_2Ag_4(O_2CH)(H)_2]^+$, $[L_2Ag_4(H)_3]^+$ and $[L_2Ag_2(H)]^+$ were all unreactive towards formic acid in the gas-phase, even at the longest reaction times studied (10 000 ms, data not shown). In contrast, the only reaction between $[dcpmAg_2(H)]^+$ and formic acid is the selective protonation of the coordinated hydride to reform the formate, $[dcpmAg_2(O_2CH)]^+$ (Fig. 4b, and step and eqn (2) of Scheme 1a), thereby closing the catalytic cycle (Scheme 1a). Under the pseudo-first order kinetic conditions used, a rate constant of $2.6 \pm 0.03 \times 10^{-10}$ cm^3 per molecules^3 per s^1 was determined, which when compared to the ADO theory rate coefficient (2.2×10^{-9} cm^3 per molecules^3 per s^1) yields a reaction efficiency of 12.0 ± 0.2%. This is approximately an order of magnitude faster than that determined previously for the bis(diphenylphosphino)methane analogue, $[dppmAg_2(H)]^+$.[1] The enhanced reactivity could be due to changes in the steric and electronic contributions from the cyclohexyl rings of dcpm compared to the phenyl rings of dppm[22] and differences in the bite angle of the phosphine ligands.[23]

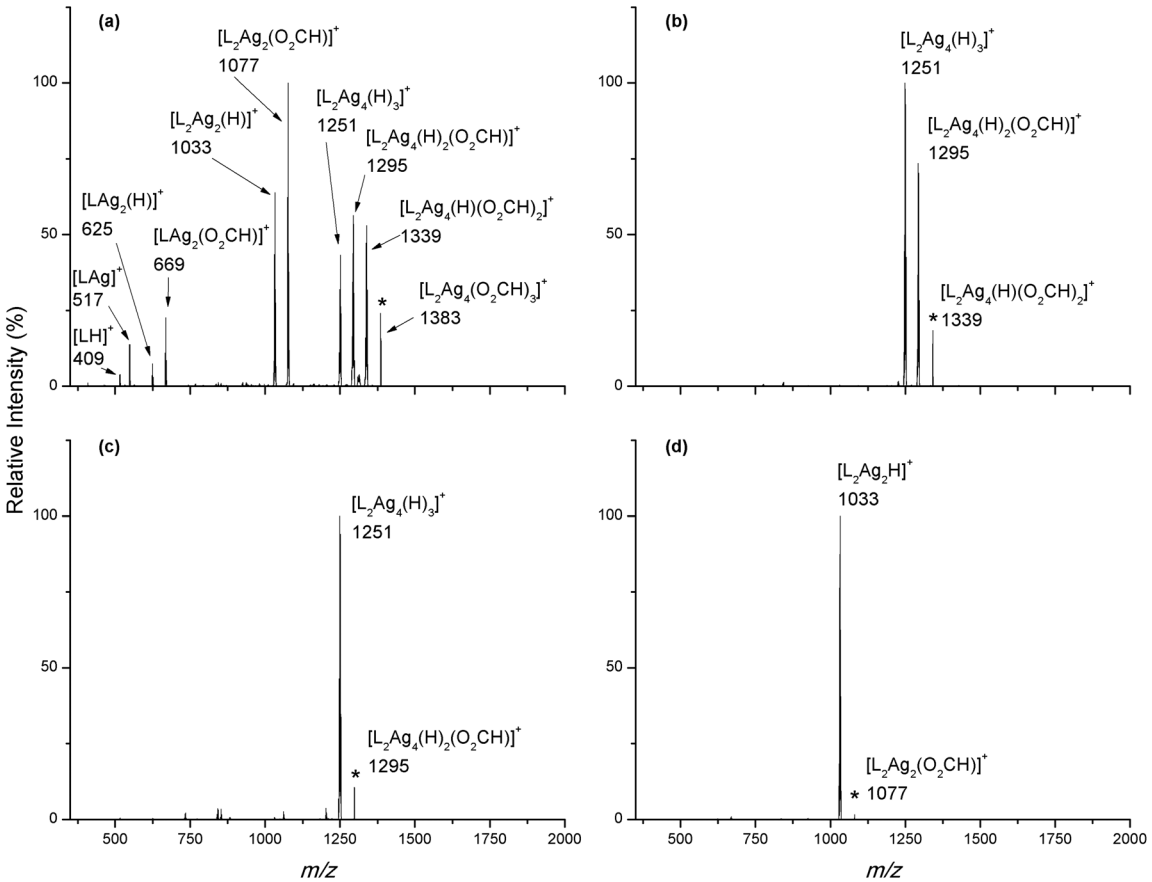

Fig. 3 LTQ MS^n experiments obtained for the collision induced dissociation of silver formato clusters: (a) $[L_2Ag_4(O_2CH)_3]^+$ (*m*/*z* 1383), (b) $[L_2Ag_4(O_2CH)_2(H)]^+$ (*m*/*z* 1339), (c) $[L_2Ag_4(O_2CH)(H)_2]^+$ (*m*/*z* 1293), and (d) $[L_2Ag_2(O_2CH)]^+$ (*m*/*z* 1078). The normalised collision energy used for each experiments was 15%. L = dcpm = bis(dicyclohexylphosphino)methane. The *m*/*z* values shown are of the most intense peak arising from isotopic abundances of the atoms.

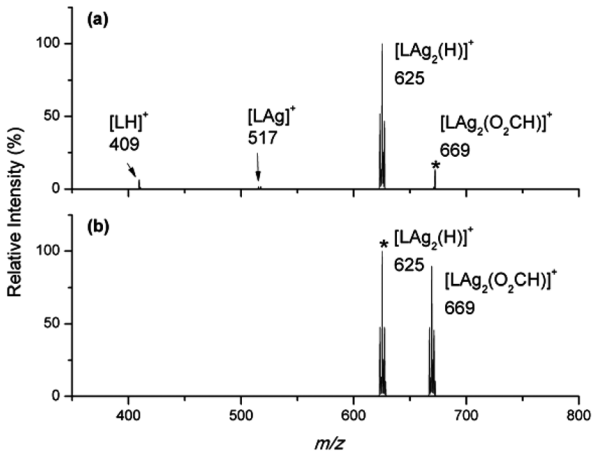

Fig. 4 Mass spectra from LTQ MS^n experiments supporting a catalytic cycle for the selective decarboxylation of formic acid: (a) CID of $[LAg_2(O_2CH)]^+$; (b) ion-molecule reaction of formic acid with $[LAg_2(H)]^+$, $[HO_2CH]_{ion\ trap}$ = 4.0 × 10^9 molecules per cm^3. Ion-activation times = 700 ms. L = dcpm = bis(dicyclohexylphosphino)methane. The *m*/*z* values shown are of the most intense peak arising from isotopic abundances of the atoms. *Represents the mass selected precursor ion.

Conclusions

This study further highlights the labile nature of coinage metal carboxylates.[7b,8] Thus while ESI/MS of an acetonitrile solution containing a mixture of $AgNO_3$: bis(dicyclohexylphosphino)methane (dcpm, L) : NaO_2CH in a molar ratio of 2 : 1 : 1 gave an abundant peak due to $[LAg_2(O_2CH)]^+$, crystallization of this solution produced a rare example of a co-crystal consisting of two discrete clusters $[(\mu_2\text{-dcpm})Ag_2(\mu_2\text{-}O_2CH)(\eta^2\text{-}NO_3)]_2$ and $[(\mu_2\text{-dcpm})_2Ag_4(\mu_2\text{-}NO_3)_4]$. Nonetheless, the dimer, $[(\mu_2\text{-dcpm})Ag_2(\mu_2\text{-}O_2CH)(\eta^2\text{-}NO_3)]_2$, within the crystal bears resemblance to the previously described gas-phase structure calculated for $[dppmAg_2(O_2CH)]^+$ (dppm = bis(diphenylphosphino)methane) (Scheme 1a).

The observation of the tetranuclear complex $[L_2Ag_4(O_2CH)_3]^+$. *via* ESI/MS provided an opportunity to see if it can also participate in a related catalytic cycle for the decarboxylation of formic acid in the gas phase (*cf.* Scheme 1a). While it does indeed undergo sequential decarboxylation reactions to provide access to the hydrides $[L_2Ag_4(O_2CH)_2(H)]^+$, $[L_2Ag_4(O_2CH)(H)_2]^+$ and $[L_2Ag_4(H)_3]^+$ (eqn (3)–(5)), significant amounts of cluster fission products are also observed

(eqn (6)–(10)). More importantly, none of these tetranuclear hydrides are reactive towards formic acid and cannot thus participate in the crucial hydride protonation step to liberate hydrogen and reform the coordinate formate (*cf.* eqn (2) and step 2 of Scheme 1a).

In contrast, $[dcpmAg_2(O_2CH)]^+$ also participates in a gas-phase catalytic cycle for the selective decomposition of formic in the gas-phase with essentially complete conversion of reactant ions to product ions and excellent selectivity for both steps, highlighting that the nature of the R group on the bisphosphine ligand is less important than the nuclearity of the cluster. The labile nature of coinage metal carboxylates suggests that there are likely to be complex equilibria and potentially multiple silver complexes in solution. While caution demands that the gas-phase results not be over-interpreted in terms of the condensed-phase *milieu*, it is nonetheless interesting to speculate that binuclear rather than tetranuclear intermediates might be associated with the observation of the evolution of CO_2 and H_2 at 65 °C from a mixture of $AgBF_4$, dppm, sodium formate and formic acid under variable temperature NMR conditions.[4] Given that a host of silver hydrides of different nuclearity can be prepared *via* ESI-MS and CID,[24] we are currently further examining how the nuclearity of ligated silver hydride complexes influences the crucial protonation step by formic acid to liberate hydrogen.

Acknowledgements

RAJO thanks the Australian Research Council for financial support DP150101388. AZ acknowledges the award of an APA scholarship.

Notes and references

1 (*a*) M. Grasemann and G. Laurenczy, *Energy Environ. Sci.*, 2012, **5**, 8171; (*b*) S. Enthaler, J. von Langermann and T. Schmidt, *Energy Environ. Sci.*, 2010, **3**, 1207.
2 (*a*) K. Saito, T. Shiose, O. Takahashi, Y. Hidaka, F. Aiba and K. Tabayashi, *J. Phys. Chem. A*, 2005, **109**, 5352; (*b*) J.-G. Chang, H.-T. Chen, S. Xu and M. C. Lin, *J. Phys. Chem. A*, 2007, **111**, 6789.
3 B. Loges, A. Boddien, F. Gärtner, H. Junge and M. Beller, *Top. Catal.*, 2010, **53**, 902.
4 A. Zavras, G. N. Khairallah, M. Krstić, M. Girod, S. Daly, R. Antoine, P. Maitre, R. J. Mulder, S.-A. Alexander, V. Bonačić-Koutecký, P. Dugourd and R. A. J. O'Hair, *Nat. Commun.*, 2016, **7**, 11746.
5 Z. Lan-Sun, Y. Hua-Hui and Z. Qian-Er, *Jiegou Huaxue*, 1992, **10**, 97.
6 G. A. Bowmaker, Effendy, J. V. Hanna, P. C. Healy, J. C. Reid, C. E. F. Rickard and A. H. White, *J. Chem. Soc., Dalton Trans.*, 2000, 753.
7 (*a*) T. S. A. Hor, S. P. Neo, C. S. Tan, T. C. W. Mak, K. W. P. Leung and R. J. Wang, *Inorg. Chem.*, 1992, **31**, 4510; (*b*) S. P. Neo, Z.-Y. Zhou, T. C. W. Mak and T. S. A. Hor, *Inorg. Chem.*, 1995, **34**, 520; (*c*) E. Szłyk, I. Szymańska, A. Surdykowski, T. Głowiak, A. Wojtczak and A. Goliński, *Dalton Trans.*, 2003, 3404.
8 (*a*) P. D. Harvey, M. Drouin and T. Zhang, *Inorg. Chem.*, 1997, **36**, 4998; (*b*) K. Jiang, D. Zhao, L.-B. Guo, C.-J. Zhang and R.-N. Yang, *Chin. J. Chem.*, 2004, **22**, 1297.
9 (*a*) G. M. Sheldrick, *Acta Crystallogr., Sect. A: Found. Crystallogr.*, 2008, **64**, 112; (*b*) G. M. Sheldrick, *Acta Crystallogr., Sect. A: Fundam. Crystallogr.*, 2015, **71**, 3.
10 L. J. Farrugia, *J. Appl. Crystallogr.*, 1997, **30**, 565.
11 L. J. Farrugia, *J. Appl. Crystallogr.*, 1999, **32**, 837.
12 (*a*) W. A. Donald, C. J. McKenzie and R. A. J. O'Hair, *Angew. Chem., Int. Ed.*, 2011, **50**, 8379; (*b*) A. K. Y. Lam, C. Li, G. N. Khairallah, B. B. Kirk, S. J. Blanksby, A. J. Trevitt, U. Wille, R. A. J. O'Hair and G. da Silva, *Phys. Chem. Chem. Phys.*, 2012, **14**, 2417; (*c*) W. A. Donald, G. N. Khairallah and R. A. J. O'Hair, *J. Am. Soc. Mass Spectrom.*, 2013, **24**, 811.
13 (*a*) T. Su and M. T. Bowers, *Int. J. Mass Spectrom. Ion Phys.*, 1973, **12**, 347; (*b*) K. F. Lim, *QCPE Bull.*, 1994, **14**, 3.
14 (*a*) A. Zavras, G. N. Khairallah, T. U. Connell, J. M. White, A. J. Edwards, P. S. Donnelly and R. A. J. O'Hair, *Angew. Chem., Int. Ed.*, 2013, **52**, 8391; (*b*) A. Zavras, G. N. Khairallah, T. U. Connell, J. M. White, A. J. Edwards, R. J. Mulder, P. S. Donnelly and R. A. J. O'Hair, *Inorg. Chem.*, 2014, **53**, 7429; (*c*) A. Zavras, A. Ariafard, G. N. Khairallah, J. M. White, R. J. Mulder, A. J. Canty and R. A. J. O'Hair, *Nanoscale*, 2015, **7**, 18129.
15 (*a*) A. D. Bond, *CrystEngComm*, 2007, **9**, 833; (*b*) M. Kriechbaum, D. Otte, M. List and U. Monkowius, *Z. Naturforsch., B: Chem. Sci.*, 2014, **69**, 1188; (*c*) M. Tabatabaeea, B.-M. Kukovecb and M. Kazeroonizadeha, *Polyhedron*, 2011, **30**, 1114.
16 (*a*) Y.-Y. Lin, S.-W. Lai, C.-M. Che, W.-F. Fu, Z.-Y. Zhou and N. Zhu, *Inorg. Chem.*, 2005, **44**, 1511; (*b*) C.-M. Che, M.-C. Tse, M. C. W. Chan, K.-K. Cheung, D. L. Phillips and K.-H. Leung, *J. Am. Chem. Soc.*, 2000, **122**, 2464.
17 A. Bondi, *J. Phys. Chem.*, 1964, **68**, 441.
18 (*a*) T. G. Gray and J. P. Sadighi, in *Molecular Metal–Metal Bonds*, ed. S. T. Liddle, Wiley-VCH Verlag GmbH & Co. KGaA, Weinheim, Germany, 2015, ch. 11, pp. 397–428; (*b*) H. Schmidbaur, *Gold Bull.*, 2000, **33**, 3; (*c*) H. Schmidbaur and A. Schier, *Chem. Soc. Rev.*, 2008, **37**, 1931; (*d*) H. Schmidbaur and A. Schier, *Angew. Chem., Int. Ed.*, 2015, **54**, 746.
19 (*a*) P.-S. Cheng, S. C. K. Hau and T. C. W. Mak, *Inorg. Chim. Acta*, 2013, **403**, 110; (*b*) S.-Q. Zang, L. Zhao and T. C. W. Mak, *Organometallics*, 2008, **27**, 2396; (*c*) Z. Chen, L. Zhang, F. Liu, R. Wang and D. Sun, *CrystEngComm*, 2013, **15**, 8877; (*d*) B. Li, R.-W. Huang, J.-H. Qin, S.-Q. Zang, G.-G. Gao, H.-W. Hou and T. C. W. Mak, *Chem. – Eur. J.*, 2014, **20**, 12416; (*e*) S. M. J. Wang and T. C. W. Mak, *Polyhedron*, 2009, **28**, 2684; (*f*) S. C. K. Hau and T. C. W. Mak, *Polyhedron*, 2013, **64**, 63; (*g*) T. Hu and T. C. W. Mak, *Organometallics*, 2013, **32**, 202.

20 E. T. Blues, M. G. B. Drew and B. Femi-Onadeko, *Acta Crystallogr., Sect. B: Struct. Crystallogr. Cryst. Chem.*, 1977, **33**, 3965.
21 N. Y. Kozitsyna, S. E. Nefedov, A. P. Klyagina, A. A. Markov, Z. V. Dobrokhotova, Y. A. Velikodny, D. I. Kochubey, T. S. Zyubina, A. E. Gekhman, M. N. Vargaftik and I. I. Moiseev, *Inorg. Chim. Acta*, 2011, **370**, 382.
22 C. A. Tolman, *Chem. Rev.*, 1977, **77**, 313.
23 Z. Freixa and P. W. N. M. van Leeuwen, *Dalton Trans.*, 2003, 1890.
24 M. Krstić, A. Zavras, G. N. Khairallah, P. Dugourd, V. Bonačić-Koutecký and R. A. J. O'Hair, ESI/MS Investigation of Routes to the Formation of Silver Hydride Nanocluster Dications $[Ag_xH_{x-2}L_y]^{2+}$ and Gas-phase Unimolecular Chemistry of $[Ag_{10}H_8L_6]^{2+}$, *Int. J. Mass Spectrom.*, DOI: 10.1016/j.ijms.2016.05.022, in press.